Precambrian Research 403 (2024) 107321

Contents lists available at ScienceDirect

Precambrian Research

journal homepage: www.elsevier.com/locate/precamres

Carbonaceous matter in ~ 3.5 Ga black bedded barite from the Dresser Formation (Pilbara Craton, Western Australia) – Insights into organic cycling on the juvenile Earth

L. Weimann [a,*], M. Reinhardt [a], J.-P. Duda [a], H. Mißbach-Karmrodt [b], H. Drake [c], J. Schönig [d], J. Holburg [e], L.B. Andreas [f], J. Reitner [a], M.J. Whitehouse [g], V. Thiel [a]

[a] University of Göttingen, Geoscience Centre, Department of Geobiology, 37077 Göttingen, Germany
[b] University of Cologne, Geobiology Group, 50674 Cologne, Germany
[c] Linnæus University, Department of Biology and Environmental Science, 39182 Kalmar, Sweden
[d] University of Göttingen, Geoscience Centre, Department of Sedimentology and Environmental Geology, 37077 Göttingen, Germany
[e] Institut für Nanophotonik Göttingen e.V., Department of Optics/Short Wavelengths, 37077 Göttingen, Germany
[f] Max Planck Institute for Multidisciplinary Science, Department of NMR-based Structural Biology, Solid-state NMR Group, 37077 Göttingen, Germany
[g] Swedish Museum of Natural History, 10405 Stockholm, Sweden

ARTICLE INFO

Keywords:
Early life
Paleoarchean
Hydrothermal
NEXAFS
NMR
SIMS

ABSTRACT

Carbonaceous matter (CM) in Archean rocks represents a valuable archive for the reconstruction of early life. Here we investigate the nature of CM preserved in ~ 3.5 Ga old black bedded barites from the Dresser Formation (Pilbara Carton, Western Australia). Using light microscopy and high-resolution Raman mapping, three populations of CM were recognized: (i) CM at the edges of single growth bands of barite crystals (most frequent), (ii) CM within the barite matrix, and (iii) CM in 50–300 μm wide secondary quartz veins that cross-cut the black bedded barite. Raman spectra of CM inside black bedded barite indicated peak metamorphic temperatures of ~ 350 °C, consistent with those reached during the main metamorphic event in the area ~ 3.3 Ga ago. By contrast, CM in quartz veins yielded much lower temperatures of ~ 220 °C, suggesting that quartz-vein associated CM entered the barite after 3.3 Ga. Near edge X-ray absorption fine structure (NEXAFS) and solid-state nuclear magnetic resonance (NMR) revealed a highly aromatic nature of the CM with a lower aliphatic content, which is in line with the relatively elevated thermal maturity. Catalytic hydropyrolysis (HyPy) did not yield any hydrocarbons detectable with gas chromatography–mass spectrometry (GC–MS). Secondary ion mass spectrometry (SIMS) based $\delta^{13}C$ values of individual CM particles ranged from − 33.4 ± 1.2 ‰ to − 16.5 ± 0.6 ‰ and are thus in accordance with a biogenic origin, which is also consistent with stromatolitic microbialites associated with the black bedded barite. Based on these results we conclude that CM at growth bands and inside the barite matrix is syngenetic and only the CM inside quartz veins, which represents a minor portion of the total CM, is a later addition to the system. Furthermore, we discuss different pathways for the input of CM into the barite-forming environment, including the cycling of biological organic material within the hydrothermal system.

1. Introduction

Life's emergence and early evolution on the young Earth are still incompletely understood. This is in part due to the complicated identification of unambiguous microbial biosignatures in our planet's oldest rocks (Lepot, 2020; Runge et al., 2022b). Solid carbonaceous matter (CM) preserved in rocks is commonly considered as being derived from organisms and thus may provide a powerful means to track life through deep geological time. However, CM preserved in early Archean rocks might as well have originated from various abiotic sources such as meteorites and/or Fischer-Tropsch type (FTT) synthesis, limiting its applicability as a deep-time biosignature (Brasier et al., 2002, 2005; De Gregorio et al., 2011; Gourier et al., 2019; Lindsay et al., 2005; McCollom et al., 1999; McCollom and Seewald, 2007; Mißbach et al., 2018; Rasmussen and Muhling, 2023; Rushdi and Simoneit, 2001; Sephton, 2002). In addition, even the least thermally altered early

* Corresponding author at: University of Göttingen, Goldschmidtstraße 3, 37077 Göttingen, Germany.
E-mail address: lena.weimann@uni-goettingen.de (L. Weimann).

https://doi.org/10.1016/j.precamres.2024.107321
Received 28 June 2023; Received in revised form 31 January 2024; Accepted 2 February 2024
Available online 17 February 2024

Archean rocks (Pilbara Craton and Barberton Greenstone Belt) have undergone prehnite-pumpellyite- to lower greenschist-facies metamorphism, complicating matters even further (Hickman, 1983; Terabayashi et al., 2003; Tice et al., 2004). This commonly results in a loss of source-specific CM features such as distinctive molecular structures or uneven distributions of homologs (cf. Mißbach et al., 2016; Vandenbroucke and Largeau, 2007). An additional problem is the potential post-depositional emplacement of CM (including hydrocarbons), which is particularly critical in early Precambrian rocks, given their long geological history (Brocks, 2011; French et al., 2015; Rasmussen et al., 2008). Despite these challenges, however, some studies were able to detect indigenous molecular compounds in early Archean rocks (Duda et al., 2018; Marshall et al., 2007; Mißbach et al., 2021; Reinhardt et al., 2024).

Important clues to the earliest life on our planet come from the 3.48 billion-year-old (Ga) Dresser Formation (Pilbara Craton, Western Australia) (van Kranendonk et al., 2008), which has been only mildly metamorphosed (prehnite-pumpellyite- to lower greenschist-facies, peak temperatures of ~ 300 °C) (Delarue et al., 2016; Hickman, 1983; Terabayashi et al., 2003). The Dresser Formation belongs to the lower part of the Warrawoona Group and is exposed in the North Pole Dome in Western Australia. It comprises a variety of lithologies, including metavolcanic and metasedimentary rocks and hydrothermal deposits (Buick and Dunlop, 1990; Djokic et al., 2017; Nijman et al., 1998; Runge et al., 2022a; van Kranendonk, 2006; van Kranendonk and Pirajno, 2004). Hydrothermal veins of the Dresser Formation mainly consist of black chert and barite and permeate pillow basalts of the older North Pole Basalt (Djokic et al., 2021; Duda et al., 2018; Lindsay et al., 2005; Nijman et al., 1998; van Kranendonk et al., 2008; van Kranendonk, 2006).

Particularly noteworthy are massive black bedded barite deposits that are spatially associated with stromatolitic microbialites consisting of metal sulfides such as pyrite and sphalerite (i.e., FeS_2 and ZnS, respectively) (Baumgartner et al., 2020; Baumgartner et al., 2019; Harris et al., 2009; Mißbach et al., 2021; Philippot et al., 2007; van Kranendonk et al., 2008; Walter et al., 1980) (Fig. 1). Regarding the origin of the black bedded barite, early studies suggested a hydrothermally driven replacement of evaporative gypsum deposits that precipitated in a shallow water marine lagoon (Barley et al., 1979; Buick and Dunlop, 1990; Dunlop and Groves, 1978). More recent work, however, has proposed direct precipitation of barite from hydrothermal fluids (Runnegar et al., 2001) in a subaquatic volcanic caldera environment (Lindsay et al., 2005; Mißbach et al., 2021; Nijman et al., 1998; Ueno, 2007; van Kranendonk et al., 2008; van Kranendonk, 2006; van Kranendonk et al., 2001; van Kranendonk and Pirajno, 2004).

Barite is highly stable across a broad range of temperature, pressure, and redox conditions and only poorly soluble (Griffith and Paytan, 2012; Hanor, 2000), making it a promising target for studies of Archean CM. Barites of the Dresser Formation contain various amounts of CM, with total organic carbon (TOC) contents of up to 0.31 wt% (Mißbach et al., 2021). Organic-rich portions show a distinct dark-grey to black color and are therefore termed "black barite" (cf. Mißbach et al., 2021). Furthermore, the black bedded barites preserve abundant primary fluid inclusions (Harris et al., 2009) containing various indigenous carbon-bearing gases such as CO_2, COS, CH_4, and numerous volatile organic molecules (Mißbach et al., 2021). This is of great geobiological relevance since these compounds may have have been available in the outflowing hydrothermal fluids and fueled microbial communities associated with the barite deposits (Mißbach et al., 2021). The origin of these organic molecules could be due to the large-scale hydrothermally driven redistribution of organic matter in early Archean subaquatic systems ("Hydrothermal Pump Hypothesis": Duda et al. (2018)). However, the nature of CM in the Dresser barites and its relation to these processes is still poorly understood.

Here we investigate the chemical and structural nature of CM in the

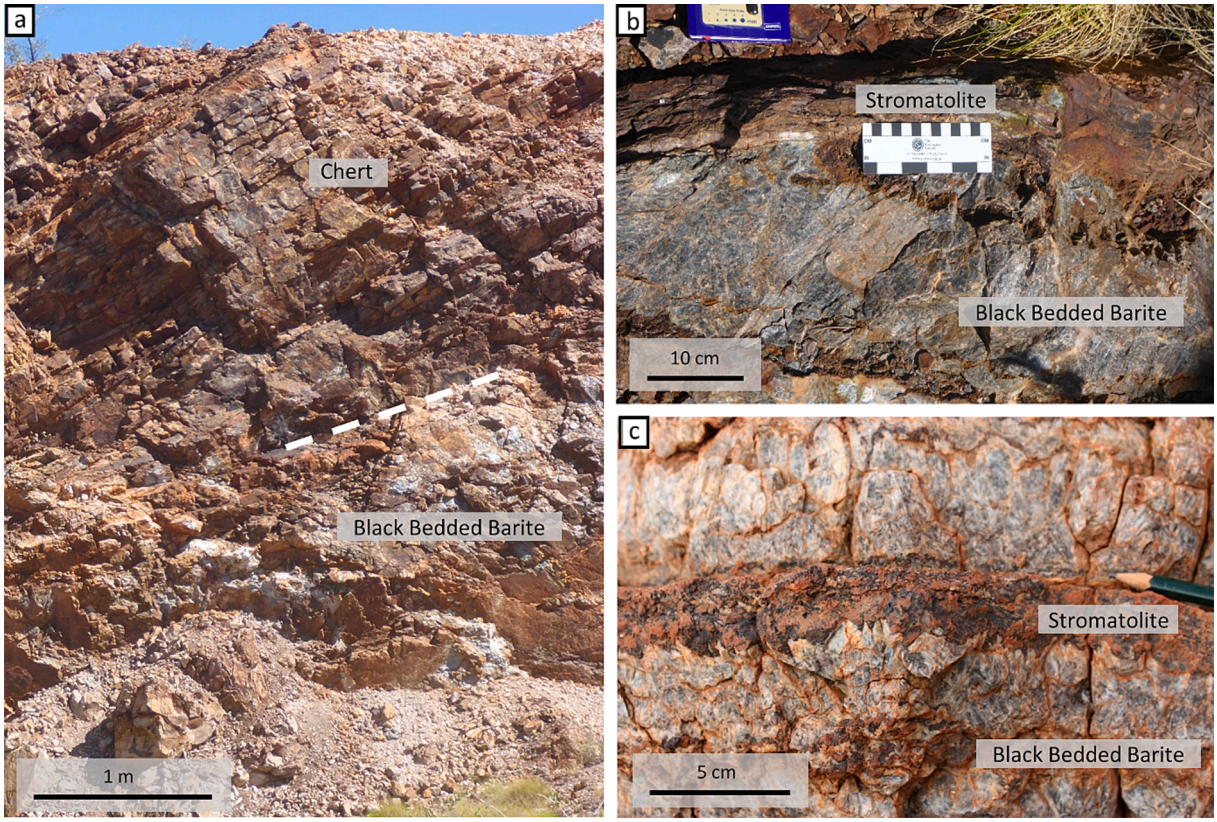

Fig. 1. Field photos from the study area. At the sampling site (a, b) and its vicinity (c), black bedded barites of the Dresser Formation contain distinct stromatolitic microbialite interbeds. The white dashed line in (a) shows the contact between chert and barite deposits. Note that reddish colors are due to surface weathering of metal sulfide minerals such as pyrite.

black bedded barites from the ~ 3.5 Ga Dresser Formation using a multifaceted analytical approach. This involves various state-of-the-art analytical techniques, including petrographic microscopy, high-resolution Raman spectroscopy, near edge X-ray absorption fine structure (NEXAFS) spectroscopy, solid-state nuclear magnetic resonance (NMR) spectroscopy, secondary ion mass spectrometry (SIMS), and catalytic hydropyrolysis (HyPy) combined with gas chromatography–mass spectrometry (GC–MS). The findings of our study help to reconstruct the nature of an early Archean habitat, including depositional processes and the influence of microbial life.

2. Methods

2.1. Sample preparation

Black bedded barite samples were taken in the Dresser Barite Mine (Pilbara Craton, Western Australia, 21° 09′ 05.2′' S, 119° 26′ 15.3′' E) (Fig. 1) from a freshly exposed wall, following established protocols using nitrile gloves, pre-cleaned tools and containers to avoid contamination during sampling and storage. Before further lab treatment, ~1.5 cm of the sample surface was removed using an acetone-cleaned saw (see Mißbach et al., 2021). All glassware and other materials used were extensively rinsed with purified organic solvents such as acetone and/or combusted (550 °C for > 4 h) to remove potential organic contaminants. The organic solvents were repeatedly distilled and tested for contamination with GC–MS as part of the lab routine. Samples were then prepared for light microscopy, Raman spectroscopy, and SIMS (polished thin sections and mounts) as well as for NEXAFS and NMR (purified CM isolates), and HyPy / GC–MS (purified powdered sample).

CM isolates were prepared by density separation in a separating funnel filled with methanol (MeOH) and *n*-hexane, as described in Reinhardt et al. (2024) (note that the isolated CM still contained traces of barite and other minerals such as pyrite). The CM isolates and powdered sample were further purified following established protocols (Brocks et al., 2003; Duda et al., 2018; Marshall et al., 2007) to remove any residual hydrocarbons that are not bound to macromolecular CM. Briefly, ~3 mg of the isolate and ~ 2 g of the powdered sample were extracted with MeOH, dichloromethane (DCM), and *n*-hexane (6 mL each; 10 min at 20 °C in an ultrasonic bath, respectively). After each step, the extracts were separated from the isolates by centrifugation (15 min at 2,000 rpm). The resulting extracts were combined, concentrated, desulfurized with active copper, and analyzed by GC–MS. The extracted isolates and powdered sample were then swelled twice by using pyridine (3 mL; 2 h at 75 °C in an ultrasonic bath) and exhaustively extracted again (3 times, procedure as above) until the yielded extracts did not contain any GC–MS detectable compounds. For H/C determination and a second NMR measurement CM was additionally baked out at 80 °C for ~ 16 h.

2.2. Raman spectroscopy

Raman spectroscopy was performed on a thin section using a WITec alpha300R fiber-coupled ultra-high throughput spectrometer. Before analysis, the system was calibrated using an integrated Xe-Hg light source. The experimental setup included a 532 nm excitation laser and a 300 lines × mm^{-1} grating covering a spectral range of 60–3900 cm^{-1} at a spectral resolution of ~ 2.7 cm^{-1}.

For two-dimensional Raman images, an automatically controlled laser power of 18 mW and a 100× long-working-distance objective (NA 0.75) were used. Spectra were collected in a 0.33 μm grid with an acquisition time of 50 ms per spectrum. The signal was amplified by an electron-multiplying charge-coupled device. Automated cosmic ray correction, background subtraction, spectral averaging/smoothing, and principal component analysis were performed using the WITec Project software.

For Raman spectrum acquisition, CM particles were individually analyzed at ≥ 16 locations per population ((i) CM at the edges of single growth bands of barite crystals, (ii) CM within the barite matrix, and (iii) CM in 50–300 μm wide secondary quartz veins that are not in areas which have been mapped (see above)). An automatically controlled laser power of 8 mW and a 50× (NA 0.8) or 100× (NA 0.9) was used. No alteration of the CM signal was observed during a preliminary series analysis using 1, 2, 4, and 8 mW. Each spectrum was acquired by two accumulations of 20 s. Automated background correction and a 4-Voigt-function fitting procedure were applied following Kouketsu et al. (2014) and considering the absence of a visible D4 band (D1, D3, G, and D2 fitting; Supplementary Fig. 1). Since a D4 band could not always be clearly identified, a sensitivity test for analyses (fitting with and without a D4 band) was performed. Deviations on the results between 4- and 5-Voigt-function fitting were insignificant with an average deviation of ~ 5 °C, which does not affect any conclusions drawn. In the manuscript we prefer a consistent evaluation with four bands (D1, D3, G, and D2) instead of a five band fit. Peak metamorphic temperatures were calculated according to Beyssac et al. (2002) and Kouketsu et al. (2014).

2.3. Near edge X-ray absorption fine structure (NEXAFS) spectroscopy

NEXAFS measurements provide an element-sensitive insight into the binding structure of CM. Measurements were performed using a table-top NEXAFS spectrometer in transmission mode with a resolution of 0.26 eV which is described in full detail in Holburg et al. (2022). CM samples were prepared via droplet deposition from a colloidal suspension of water and isopropanol onto a 100 nm thick silicon nitride membrane to create an optical thin and homogeneous layer of CM. Spectra were then recorded by integrating over 750 pulses in 2.5 min and evaluated according to Lambert-Beer's law, yielding the absorbance.

2.4. Solid-state nuclear magnetic resonance (NMR) spectroscopy

Hahn-echo (Hahn, 1950) ^{13}C NMR spectra were recorded using a 800 MHz Bruker spectrometer equipped with a 1.3 mm H/C/N Bruker narrow bore probe. The 90 degree ^{13}C excitation pulse was 4 μs, the Hahn-echo period was two rotor periods (36.36 μs), and the magic-angle spinning frequency was 55 kHz. To attenuate dipolar line broadening, proton decoupling of ~ 12 kHz swept two pulse phase modulation (TPPM) (Thakur et al., 2006) was applied throughout the Hahn-echo and detection periods. The inter-scan delay was 20 s. The time-domain data was multiplied by a 2000 Hz broad exponential function prior to Fourier transformation. Two measurements on CM isolates (see 2.2) were performed. The total acquisition time was ~ 10 days.

2.5. Secondary ion mass spectrometry (SIMS)

SIMS was performed at the Swedish Museum of Natural History, Stockholm (NordSIM facility). Black bedded barite fragments were mounted in epoxy and polished. The fragments were carefully placed in epoxy and sample surfaces were screened with scanning electron microscopy (SEM) for suitable analysis spots and to avoid spot placement in epoxy. Carbon isotopes from the CM particles were analyzed with a primary ion beam of 10 μm and 1–2 μm depth dimension using a CAMECA IMS1280 instrument with settings described in Hickman-Lewis et al. (2020), including multicollection at a mass resolution of 2460 (^{12}C channel, ion counter) and 4000 (^{13}C channel). Here, however, a Faraday detector was used for the ^{13}C channel instead of an ion counter. To sputter targets, a 5 μm raster and a ~ 1 nA Cs^+ primary beam were used and charge compensation was maintained by a low energy electron gun.

To check for the instrumental mass bias, an in-house pyrolyzed graphite standard was used as a reference (C-pyr2; $\delta^{13}C = -35.7$ ‰ ± 0.3 ‰ cross calibrated against another pyrolyzed graphite C-pyr1 with $\delta^{13}C = -30.8$ ‰ (Nemchin et al., 2008)). The reproducibility was 0.25

‰ (SD), determined during two sessions. Furthermore, instrumental mass fractionation of carbon isotopes during CM analysis with SIMS occurs due to a matrix effect dependent on the H/C ratio of the CM (Sangély et al., 2005). This instrumental fractionation was corrected by analyzing two pyrobitumen reference materials from Kallmora and Grängesberg, Sweden, with known H/C (Welin, 1966) and $\delta^{13}C$ composition (−30.1 ± 0.2 ‰ and − 29.1 ± 0.2 ‰; determined on a Flash 2000 elemental analyzer coupled to a Delta plus XP isotope ratio mass spectrometer via a ConFlo III interface), and by analyzing the H/C ratio of the barite CM via combustion elemental analysis (Elementar MICRO cube elemental analyzer). To correct for the instrumental bias (Δ_{inst}), values for the H/C effect were determined, assuming the same linear behavior as reported in Sangély et al. (2005). Δ_{inst} was calculated as follows: Δ_{inst} [‰] = 1000 * ln(α_{inst}), where $\alpha_{inst} = (^{13}C/^{12}C_{meas}) / (^{13}C/^{12}C_{actual})$. $^{13}C/^{12}C_{meas}$ was measured by SIMS and $^{13}C/^{12}C_{actual}$ was measured by conventional bulk sample mass spectrometry (see Reinhardt et al., 2024). A session specific H/C-correction was then applied using Δ_{inst} and the H/C ratios of the reference pyrobitumens, pyrolyzed graphite, and CM.

2.6. Catalytic hydropyrolysis (HyPy)

HyPy allows a gentle release of covalently bound hydrocarbons from macromolecular organic matter by progressive heating under high pressure and a permanent hydrogen atmosphere (Love et al., 1995; Meredith et al., 2014). The HyPy rig (Strata Technology Ltd., Nottingham, UK) was operated at a hydrogen pressure of 150 bar and a hydrogen sweep gas flow of 6 L/min. Prior to each sample run, the HyPy reactor was cleaned by rapid heating to 520 °C at 300 °C min^{-1}. To monitor potential contamination, both gas and instrument blanks were performed before and after sample runs.

Sample runs were performed in duplicate, each using ~ 2 g of black bedded barite powder. The samples were mixed with ~ 100 mg ammonium dioxydithiomolybdate catalyst (to increase product yields) and ~ 100 mg silica gel (to prevent clogging of the system). HyPy was then conducted using a two-step approach (Brocks et al., 2003; Duda et al., 2018; Marshall et al., 2007; Reinhardt et al., 2024). The first step included heating to 250 °C at 300 °C min^{-1} and to 330 °C at 8 °C min^{-1} (held for 10 min) to release any residual compounds not bound to macromolecular CM. In the second step, the sample was heated to 520 °C at 8 °C min^{-1} to release covalently bound molecules. The products were trapped on a dry-ice-cooled silica gel trap (Meredith et al., 2004). After each run, products were eluted from the silica gel with DCM, desulfurized with activated copper, and analyzed by GC–MS.

2.7. Gas chromatography–mass spectrometry (GC–MS)

HyPy products were analyzed using a Thermo Trace 1310 GC coupled to a Thermo TSQ Quantum Ultra triple quadrupole MS. The GC was equipped with a TriPlus RSH autosampler, a splitless injector (kept at 80 °C), and a Phenomenex Zebron ZB-5MS fused silica capillary column (30 m length, 250 μm internal diameter, 0.25 μm film thickness). The GC temperature was initially set at 80 °C (held for 1 min) and then ramped to 310 °C at 5 °C min^{-1} (held for 20 min). Helium was used as carrier gas at a constant flow of 1.5 mL min^{-1}. Electron ionization mass spectra were recorded in full scan mode (50–600 *m/z*) at a scan time of 0.4 s, solvent delay of 6 min, and an electron energy of 70 eV. Sensitivity and system blindness were frequently controlled by reference measurements of a fatty acid methyl ester (FAME) standard. Compounds were identified by the retention time of peaks and mass spectra. The cleanliness of the GC–MS system was routinely controlled by analysis blanks throughout the project.

3. Results

3.1. Petrography

At the sampling site, the massive black bedded barite deposit is overlain by bedded chert (Fig. 1a). Black bedded barites here and elsewhere in the study area exhibit a coarse crystalline texture and contain distinct cm to dm thick interbeds of stromatolitic microbialites (Fig. 1b, c).

The black bedded barite is made up of partly orthorhombic barite crystals that overgrow each other (Fig. 2a) and show no indications for post-depositional recrystallization. Single barite crystals (up to 2 mm) are separated by clearly discernible growth bands. The barite matrix of single crystals consists of finely crystalline and homogenous barite. Secondary quartz veins cross-cut the black bedded barite matrix (Fig. 2), but account for only a small portion of the rock volume (~5 vol%).

Within the analyzed samples, irregularly shaped particles of CM (up to 20 μm) occur along barite crystal growth bands, within the matrix of barite crystals, and within secondary quartz veins (listed in decreasing order of abundance; Fig. 2). The CM particles are often associated with mineral inclusions, in particular carbonates and sulfides. Furthermore, the barite contains abundant small fluid inclusions (~10 μm), which are mainly composed of fluid and vapor phases but partly also contain CM. Previous studies have shown that the fluid inclusions preserve diverse carbon-bearing volatiles (Harris et al., 2009; Mißbach et al., 2021).

3.2. Raman spectroscopy

Raman spectra of CM particles show a D1 band at ~ 1354 cm^{-1} and a G + D2 band at ~ 1608 cm^{-1}. Notably, Raman band intensities of CM particles associated with barite crystals systematically differ from those occurring within quartz veins (D1 > G + D2 and D1 < G + D2, respectively) (Fig. 3a-c).

Peak metamorphic temperatures calculated according to Beyssac et al. (2002) range from 287 to 346 °C (average 310 °C, n = 19; CM particles along crystal growth bands), through 285–370 °C (average 319 °C, n = 16; CM particles within crystals), to 283–370 °C (average 313 °C, n = 19; CM particles within secondary quartz veins) with an uncertainty of ± 50 °C (Supplementary Fig. 2). In comparison, peak metamorphic temperatures calculated after Kouketsu et al. (2014) range from 183 to 370 °C (average 345 °C, n = 19; CM particles along crystal growth bands), through 263–366 °C (average 315 °C, n = 16; CM particles within crystals), to 107–271 °C (average 216 °C, n = 19; CM particles within secondary quartz veins) (Fig. 3d) with an uncertainty of ± 30 °C. Considering the temperature estimates and the calibration range of > 330 °C for the thermometer after Beyssac et al. (2002), solely temperature estimates calculated after Kouketsu et al. (2014) are considered in the following.

3.3. NEXAFS and NMR

NEXAFS spectra of isolated CM show two peaks at 285.3 eV and 287.0 eV (Fig. 4c), representing C=C bonds in aromatic rings and C–C bonds in aliphatic moieties, respectively (De Gregorio et al., 2011). This is in good accordance with peaks at 140 ppm and 25 ppm in NMR spectra (Fig. 4a, b) (Cao et al., 2013; Miknis et al., 1981), which further confirms the presence of aromatic and aliphatic components in the isolated CM. As peak areas in NMR and NEXAFS spectra are roughly proportional to the quantity of the respective fraction, the relative proportion of aromatic components in the isolated CM can be estimated to be 65.0 % and 68.0 % for the first and second NMR measurement, respectively (Fig. 4a, b), and 67.3 % for the NEXAFS data (Fig. 4c).

3.4. SIMS

Microscale SIMS analyses on individual CM particles provided $\delta^{13}C$

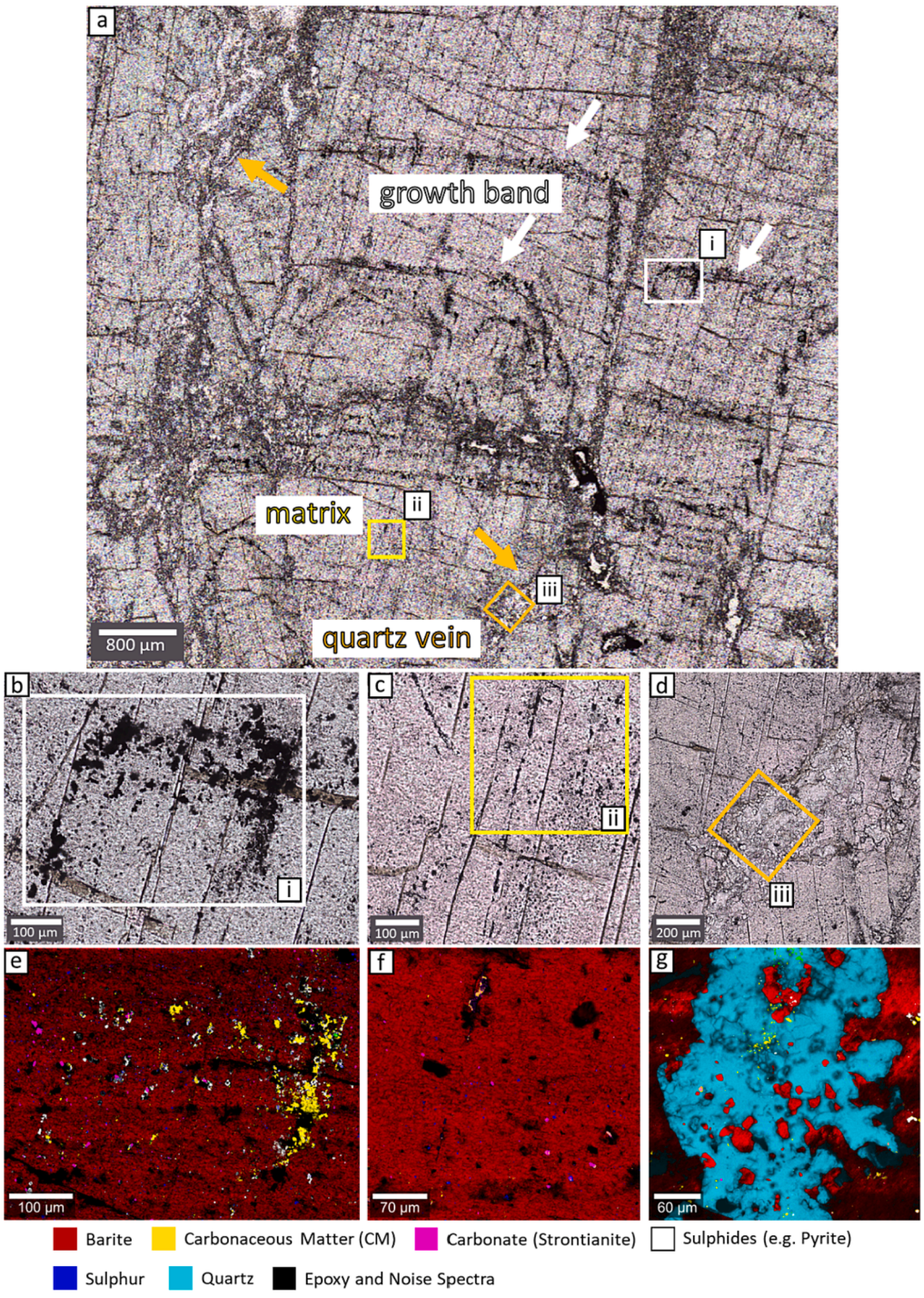

Fig. 2. Populations of CM in black bedded barite of the Dresser Formation. (a) Transmitted light photomicrograph of black bedded barite showing characteristic crystal growth bands (white arrows). Some quartz veins crosscut the barite (orange arrows). Rectangles (i)–(iii) in (a) show positions for Raman mappings shown in (b–d). Raman mappings of a growth band (e), the barite matrix (f), and a quartz vein (g), with CM shown in yellow.

values between − 33.4 ± 1.2 ‰ and − 16.5 ± 0.6 ‰ (errors represent 2σ values) (Fig. 5, Supplementary Table 1). The broad $\delta^{13}C$ range was observed in all CM particles associated with black bedded barite, including those in the matrix and the contact zone between growth zones. Double measurements on single CM particles in different spot locations show values that differ significantly from each other (~2–8 ‰). The mean H/C value of the CM isolate was 0.5 (Supplementary Table 1).

3.5. GC–MS of HyPy pyrolysates

The low and high-temperature HyPy pyrolysates from both runs only contained minor traces of *n*-alkanes, which were also present in the blank runs (Supplementary Fig. 3).

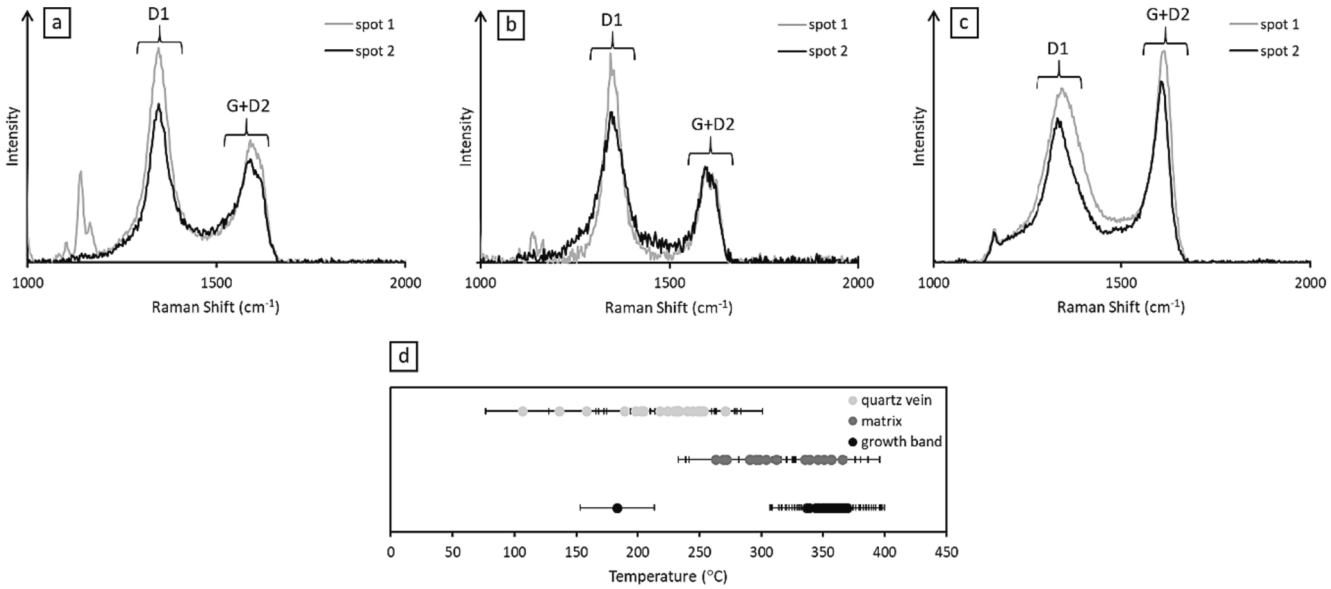

Fig. 3. Raman analysis of CM in barites of the Dresser Formation. Raman spectra for CM (a) at growth bands, (b) inside the barite matrix, and (c) inside quartz veins. Maximum metamorphic temperatures (T_{max}) for CM (d) calculated according to Kouketsu et al. (2014). Average temperatures (uncertainty ± 30 °C) are 345 °C at growth bands (n = 19), 315 °C inside the matrix (n = 16), and 216 °C inside quartz veins (n = 19). Note that the thermometer used was calibrated for the temperature range of 150–400 °C (Kouketsu et al., 2014); measuring points outside this range must be interpreted with caution.

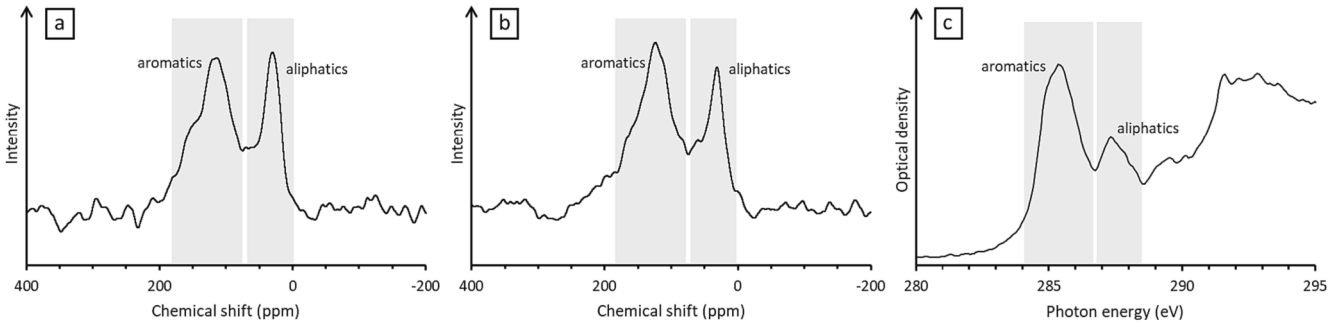

Fig. 4. Structural analysis of CM in barites of the Dresser Formation using NMR (a, b) and NEXAFS (c). The fraction of aromatic carbon was estimated based on peak areas: (a) 68.0 %, (b) 65.0 % and (c) 67.3 %.

4. Discussion

4.1. Syngeneity of CM to the host rock

Most of the CM in the black bedded barite is concentrated along crystal growth bands or occurs finely distributed within the mineral matrix. Because the barite shows no indications for later recrystallization, the CM appears to be syngenetic with the host rock. However, minor occurrences of CM within secondary quartz veins (Fig. 2) suggest migration or transport of organic matter after precipitation of the black bedded barite. Raman-based peak metamorphic temperatures calculated after Kouketsu et al. (2014) reveal different temperatures for black bedded barite (along crystal growth bands and in the mineral matrix) and quartz-vein-associated CM (~345 °C and ~ 216 °C, respectively; Fig. 3), indicating a different thermal history. The temperatures for CM associated with the black-bedded barite are in line with the metamorphic history of the Pilbara Craton, which was only mildly metamorphosed by the intrusion of granitoid melts ~ 3.3 Ga ago (lower greenschist-facies, ~300 °C) (Delarue et al., 2016; Hickman, 1983; Terabayashi et al., 2003). These temperature estimates are also consistent with those found for CM from hydrothermal chert veins of the Dresser Formation in the same area (up to 350 °C) (Ueno et al., 2004). Nevertheless, calculated temperatures can reflect the thermal alteration of CM prior to or during emplacement (Olcott Marshall et al., 2012). Indeed, CM in hydrothermal environments might experience peak temperatures that are not exceeded during post-depositional heating. The in-situ thermal alteration of CM in hydrothermal environments is a well-known phenomenon and was, for instance, demonstrated for Pleistocene cherts from Lake Magadi, where Raman-based temperatures vary from 40 °C to 440 °C (Reinhardt et al., 2019). In other studies two CM phases with different peak metamorphic temperatures were found in the 3.46 Ga old Apex Chert, indicating syngenetically deposited CM and CM introduced by post-metamorphic hydrothermal fluids (Rouillard et al., 2021; Sforna et al., 2014). Our data, which shows two distinct temperature populations similar to the Apex Chert studies, suggests that the CM in the black bedded barite is likely syngenetic, while the CM in the secondary quartz veins was emplaced later than 3.3 Ga ago.

The exact origin of the CM in secondary quartz veins is difficult to constrain. It may derive from petroleum-like fluids that formed via thermal cracking of macromolecular organic matter in associated deposits. These products would then have migrated into the barite after the peak metamorphic overprint at ~ 3.3 Ga. Another, not necessarily contradictory possibility is the direct transport of organic particles by post-metamorphic hydrothermal fluids, as it has been proposed for CM in chert veins of the Apex Chert (Olcott Marshall et al., 2012; Rouillard et al., 2021; Sforna et al., 2014).

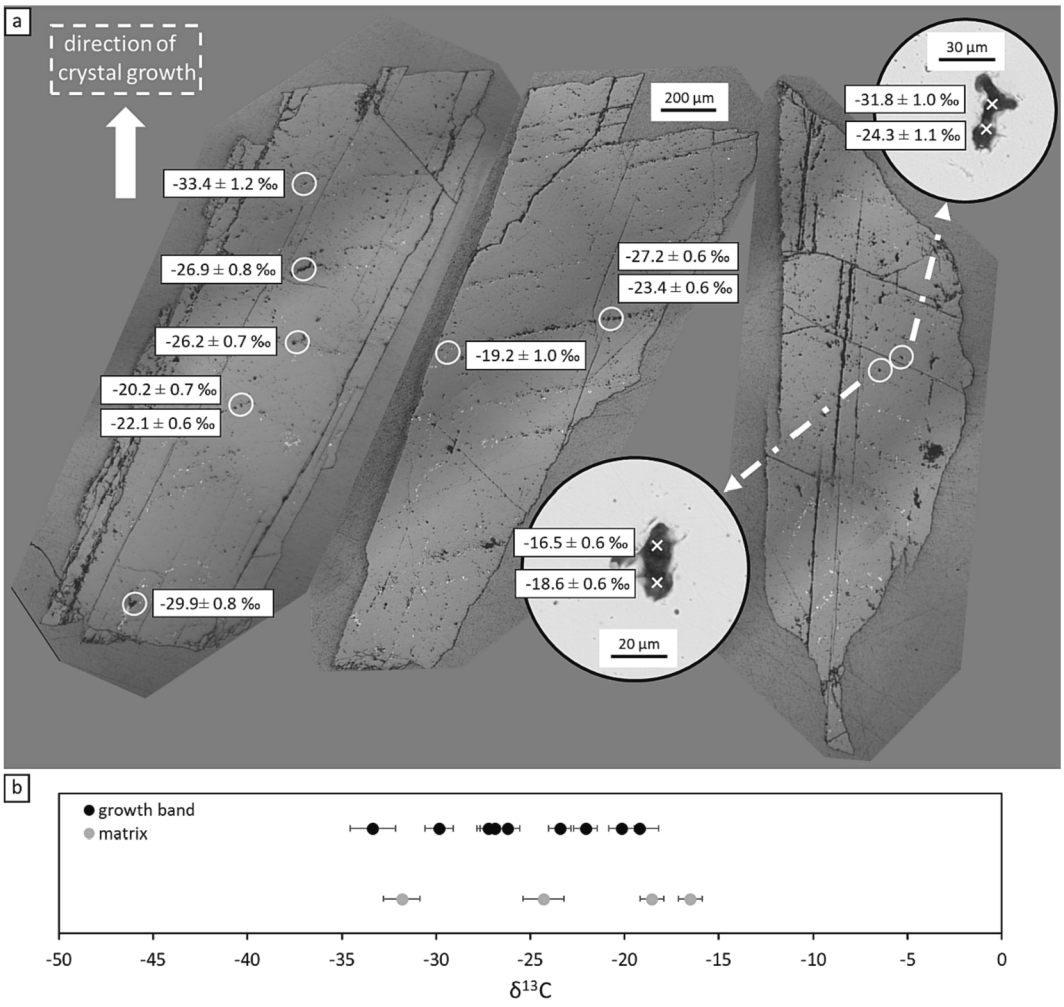

Fig. 5. Micro-scale $\delta^{13}C$ measurements of CM in barites of the Dresser Formation via SIMS. (a) SEM image showing barite fragments, including CM inclusions along growth bands or within the barite matrix. Micro-scale $\delta^{13}C$ measurements were performed on CM flakes within white circles. (b) Summary of $\delta^{13}C$ values from CM along growth bands (n = 9) and inside the barite matrix (n = 4). 2σ errors are shown.

4.2. Chemical and structural characteristics of CM

Diagenesis and thermal maturation of organic matter result in a loss of hydrogen through condensation and aromatization (Tissot and Welte, 1984). Hence, the low H/C ratio of CM in the analyzed sample (0.5) is well in line with the elevated thermal maturity of the Dresser Formation. More specific, semi-quantitative analyses with NEXAFS and NMR support this view in showing that the CM mainly consists of aromatic hydrocarbons (means of 66.8 ± 2.6 %; Fig. 4) with a lower aliphatic component. This is in good accordance with HyPy studies on chert samples from the Dresser Formation and the ~ 3.4 Ga Strelley Pool Formation (also Pilbara Craton), which demonstrated that Paleoarchean rocks from that region may indeed preserve CM-bound aromatic and aliphatic (*n*-alkyl-) moieties (Duda et al., 2018; Marshall et al., 2007). Other studies that used NEXAFS/X-ray absorption near-edge structure spectroscopy (XANES) to analyze CM from different deposits in the Pilbara Craton also show a prominent peak for aromatic bonds, but only trace amounts of aliphatics (Alleon et al., 2019; Alleon et al., 2018; Igisu et al., 2022). These studies have analyzed the CM on the microscale rather than the bulk level (this study) which may explain such differences. The absence of detectable aliphatic hydrocarbons in HyPy products (Supplementary Fig. 3) could result from (i) insufficient sample amounts, (ii) a prevalence of moieties not pyrolysable by HyPy, and/or (iii) compounds with molecular masses outside the analytical window of GC–MS. In particular, potential low-molecular weight but GC–MS amenable hydrocarbons in HyPy products might have been lost during sample work-up (e.g., through evaporation during drying of fractions: Ahmed and George (2004)). This underpins the value of techniques such as NEXAFS and NMR as complementary tools for the analysis of ancient CM.

4.3. Depositional environment and CM origin

The Dresser black bedded barite has originally been interpreted to originate from replacement of primarily formed gypsum pseudomorphs (Barley et al., 1979; Buick and Dunlop, 1990; Dunlop and Groves, 1978). However, this is no longer consistent with the current view that the black bedded barite is a primary precipitate (Runnegar et al., 2001). Black bedded barite crystals most likely grew inside an active volcanic caldera due to hydrothermal fluid circulation (Lindsay et al., 2005; Nijman et al., 1998; Ueno, 2007; van Kranendonk et al., 2008; van Kranendonk, 2006; van Kranendonk et al., 2001; van Kranendonk and Pirajno, 2004). These fluids penetrated the crust through growth faults and transported barium, which precipitated as barite in veins close to the surface or, after outflow, in the stratiform layers studied here (van Kranendonk, 2011).

The results of our study support the reconstruction of processes that have been involved in the formation of the black bedded barite deposits (Fig. 6). The enrichment of CM along crystal growth bands might indicate an accumulation of organic particles from the water column on

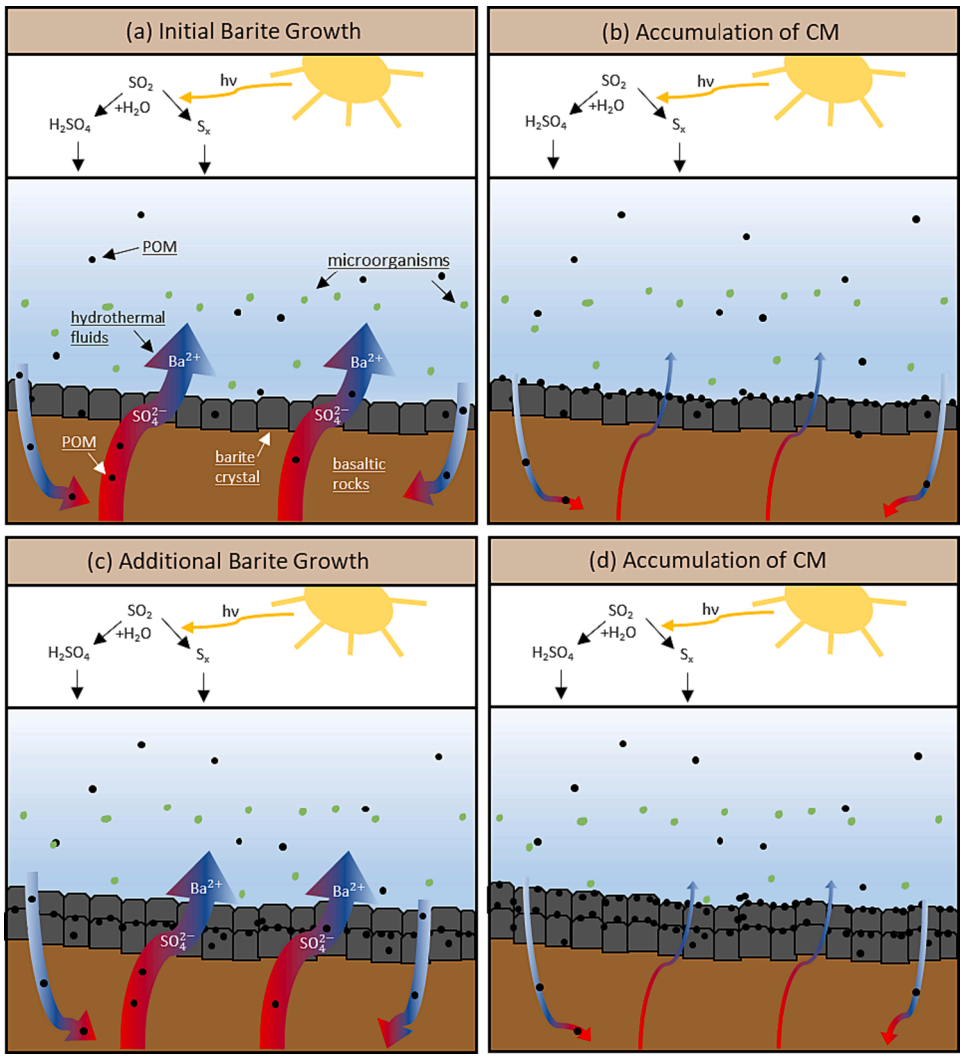

Fig. 6. Depositional model for black bedded barite of the Dresser Formation (Pilbara Craton, Western Australia), focusing on the fluid-organic-dynamics (i.e. stromatolitic microbialites and younger chert units are not included). (a) Hydrothermal fluids supply Ba^{2+} and perhaps SO_4^{2-} to the surface environment, resulting in the precipitation of barite at the sediment–water interface (note atmospheric SO_2 as alternative, yet not contradictory source of sulfate input). POM mainly from biological sources is settling from the water column and becomes incorporated in the precipitating barite. (b) In phases of low hydrothermal fluid flow, settling POM accumulated on top of the existing barite surfaces. (c, d) Through alternating hydrothermal activity, POM would repeatedly be incorporated within barite crystals (c) or concentrated in barite crystal growth zones (d).

crystal surfaces at the water–sediment interface (Fig. 6). This requires that the barite crystals were exposed for some time during periods of less intense fluid flow and reduced mineral precipitation rates (Fig. 6b, d). During pulses of intensified hydrothermal fluid flow, barite precipitation rates increased and CM particles settling from the water column became evenly incorporated into the growing crystals (Fig. 6a, c). The varying rates of barite precipitation and crystallization could explain the dilution of CM in the matrix and its accumulation at the growth interfaces. During phases of low and cooler hydrothermal fluid flow, biofilms and microbial mats thrived on top of the black bedded barite deposits, as indicated by the interlayered stromatolitic microbialites (Fig. 1b, c). During such periods, seeping fluids may have provided a continuous carbon and energy source for these benthic microbial communities (Mißbach et al., 2021). Another plausible (and non-exclusive) scenario to explain the difference in CM appearance between matrix and growth interfaces is the reduced incorporation of solid particles (including CM) during crystal growth, resulting in an expulsion of the particles towards the surrounding medium and subsequent enrichment at the crystal surface (cf. Asenath-Smith et al., 2012; Chernov, 1984; Shtukenberg et al., 2017). The latter might also apply to other impurities present in the black bedded barite as solid inclusions (carbonates, sulfides; see 3.4).

A central question concerns the origin of the CM in the black bedded barites. One possibility is that the CM represents particulate organic matter (POM) from microorganisms living in the water column or on the barite-water interface. Additionally, experiments have shown that dissolved organic matter (DOM) in hydrothermal systems is thermally altered and could partly be transformed to POM (Hawkes et al., 2016, their fig. 7). DOM and POM could have been reworked by getting entrained into the hydrothermal system and later released to the water column again (Duda et al., 2018). Such hydrothermal cycling has also been proposed for POM expelled with fluids from modern marine hydrothermal systems (Lin et al., 2021). Given that the Archean ocean was certainly more reducing than today (Rasmussen and Buick, 1999), more organic compounds may have survived these cycling processes.

There is ample evidence that the Dresser environment was teeming with microbial life (Djokic et al., 2017; van Kranendonk et al., 2018; van Kranendonk, 2007), and it has been proposed that organic matter produced by organisms was altered and redistributed through hydrothermal circulation (Duda et al., 2018). Hence, it is plausible to assume that the CM particles have a biological origin, at least partially. $\delta^{13}C$

signatures of barite-associated CM range between − 33.4 ‰ and − 16.5 ‰ (mean − 24.6 ± 10 ‰) (Fig. 5), which is consistent with previously reported $\delta^{13}C$ values for CM in the bulk black bedded barite (mean of − 27.6 ± 0.6 ‰: Mißbach et al., 2021). Mantle CO_2, the initial source for carbon in the water column, ranges between − 7 ‰ and − 5 ‰ (Des Marais and Moore, 1984), which is right in the $\delta^{13}C$ range of CO_2 in primary fluid inclusions from grey barite of the Dresser Formation (Mißbach et al., 2021). CM from the black bedded barite is thus depleted in $\delta^{13}C$ compared to mantle CO_2 by > 10 ‰ which is in full agreement with a fractionation through biological carbon fixation (Schidlowski, 1988).

Further, the observed spread in $\delta^{13}C$ for individual barite-associated CM particles (~17 ‰) is in line with findings from other Archean units and might reflect individual metabolisms characterized by different pathways of carbon fixation (Morag et al., 2016; Reinhardt et al., 2024). For instance, lower $\delta^{13}C$ values may be expected for CM originating from organisms using the acetyl coenzyme A pathway (e.g. Preuß et al., 1989) as for carbon fixation using the Calvin cycle (e.g. Pearson, 2010). Another possible explanation for the internal $\delta^{13}C$ variation observed within single CM particles (Fig. 5) is the selective preservation of different cell constituents, since microbial membrane components can be depleted in ^{13}C up to 10 ‰ as compared to intracellular organics (Lepot et al., 2013; Sakata et al., 1997). Alternatively, hydrothermal alteration could shift the $\delta^{13}C$ to heavier values by (i) the loss of isotopically light low molecular weight compounds (like CH_4) by thermal cracking and/or by (ii) high temperature isotope exchange with dissolved CO_2 or other carbon bearing molecules, e.g. via several successive hydrothermal alteration cycles before final entrapment (van Zuilen et al., 2007).

It has been suspected that parts of organic matter in the Pilbara Craton might be of abiotic origin (Lindsay et al., 2005; Mißbach et al., 2021; Rasmussen and Muhling, 2023). Indeed, FTT synthesis in the laboratory has been demonstrated to result in the formation of various biomarker-like lipids (Mißbach et al., 2018), and these potentially show $\delta^{13}C$ values in the range of biological organic matter (Horita and Berndt, 1999; McCollom and Seewald, 2006). However, studies on modern hydrothermal settings so far reported only small molecules (C_1–C_4) as putative FTT synthesis products, not organic compounds of higher molecular weight or particles (Charlou et al., 2002; Proskurowski et al., 2008). Experimental work suggested the possible formation of polymers from FTT products under hydrothermal conditions, but it remained unclear whether any more complex (insoluble) macromolecular organic matter can be formed (Mißbach et al., 2018). Furthermore, geochemical modeling indicates that the potential for abiotic synthesis of organic compounds in hydrothermal systems is strongly dependent on the hydrogen content of the fluids involved (Shock and Schulte, 1998). FTT is thus favored by serpentinization reactions that act as hydrogen sources in natural hydrothermal systems (Berndt et al., 1996). Although no indications for large-scale serpentinization of the underlying komatiitic basalt in the Dresser Formation has been observed during fieldwork, it cannot be fully excluded that POM of abiotic origin was introduced by hydrothermal fluids from elsewhere. Nevertheless, the combined evidence including (i) the lack of indications for serpentinization, (ii) $\delta^{13}C$-values of the barite-hosted CM, (iii) distinct molecular biosignatures in hydrothermal cherts from the Dresser Formation (Duda et al., 2018), and (iv) the interbedding of the black bedded barites with stromatolites (Fig. 1b, c; Mißbach et al., 2021) strongly argues for a biological origin of the barite-hosted CM.

Conclusion

We demonstrate that most CM in black bedded barite of the ~ 3.5 Ga Dresser Formation is syngenetic to the host rock. However, subordinate CM associated with secondary quartz veins indicates small scale introduction of organic matter after the main metamorphic event at ~ 3.3 Ga. This secondary CM can be distinguished from the indigenous (i.e. barite-hosted) population using a Raman thermometer calibrated for temperatures < 300 °C. Our findings suggest that hydrothermal fluid pulses controlled the deposition of the black bedded barite and the accumulation of organic matter along crystal growth bands therein. Barite-associated CM mainly consists of aromatic networks, but also contains an aliphatic component, supporting that such moieties can survive despite high thermal maturities. $\delta^{13}C$ values observed for individual CM particles (between − 33.4 ‰ and − 16.5 ‰) are consistent with an origin from biological sources. The isotopic variation likely results from different metabolic pathways and/or varying degrees of hydrothermal alteration.

CRediT authorship contribution statement

L. Weimann: Conceptualization, Data curation, Formal analysis, Investigation, Methodology, Visualization, Writing – original draft, Writing – review & editing. **M. Reinhardt:** Conceptualization, Formal analysis, Methodology, Supervision, Writing – review & editing. **J.-P. Duda:** Conceptualization, Funding acquisition, Project administration, Supervision, Writing – review & editing. **H. Mißbach-Karmrodt:** Data curation, Methodology, Writing – review & editing. **H. Drake:** Formal analysis, Funding acquisition, Methodology, Writing – review & editing. **J. Schönig:** Data curation, Formal analysis, Methodology, Writing – review & editing. **J. Holburg:** Data curation, Formal analysis, Methodology, Writing – review & editing. **L.B. Andreas:** Data curation, Formal analysis, Methodology, Writing – review & editing. **J. Reitner:** Data curation, Funding acquisition, Project administration, Supervision, Writing – review & editing. **M.J. Whitehouse:** Data curation, Formal analysis, Methodology, Writing – review & editing. **V. Thiel:** Conceptualization, Data curation, Funding acquisition, Project administration, Supervision, Writing – review & editing.

Declaration of competing interest

The authors declare that they have no known competing financial interests or personal relationships that could have appeared to influence the work reported in this paper.

Data availability

Data will be made available on request.

Acknowledgments

We thank three anonymous reviewers for very constructive comments and suggestions. We furthermore thank W. Dröse, A. Hackmann, M. Rittmeier, B. Röring (all University of Göttingen), and S. Gustafsson (Chalmers University of Technology) for support in the lab. This work was funded by the Deutsche Forschungsgemeinschaft (DFG) SPP 1833 “Building a Habitable Earth” (276836342, Du 1450/3-1, Du 1450/3-2; Re 665/42-2; Th 713/13-2), the DFG Emmy Noether Programme (422423310, Du 1450/7-1), the DFG project 434531747, the Swedish Research Council (contract 2021-04365), and Formas (contract 2020-01577) as well as financially supported by the MPI-NAT. This is NordSIMS contribution 743.

Appendix A. Supplementary material

Supplementary data to this article can be found online at https://doi.org/10.1016/j.precamres.2024.107321.

References

Ahmed, M., George, S.C., 2004. Changes in the molecular composition of crude oils during their preparation for GC and GC–MS analyses. Org. Geochem. 35, 137–155. https://doi.org/10.1016/j.orggeochem.2003.10.002.

Alleon, J., Bernard, S., Le Guillou, C., Beyssac, O., Sugitani, K., Robert, F., 2018. Chemical nature of the 3.4 Ga Strelley Pool microfossils. Geochem. Persp. Let. 7, 37–42. https://doi.org/10.7185/geochemlet.1817.

Alleon, J., Flannery, D.T., Ferralis, N., Williford, K.H., Zhang, Y., Schuessler, J.A., Summons, R.E., 2019. Organo-mineral associations in chert of the 3.5 Ga Mount Ada Basalt raise questions about the origin of organic matter in Paleoarchean hydrothermally influenced sediments. Sci. Rep. 9, 16712. https://doi.org/10.1038/s41598-019-53272-5.

Asenath-Smith, E., Li, H., Keene, E.C., Seh, Z.W., Estroff, L.A., 2012. Crystal Growth of Calcium Carbonate in Hydrogels as a Model of Biomineralization. Adv. Funct. Mater. 22, 2891–2914. https://doi.org/10.1002/adfm.201200300.

Barley, M.E., Dunlop, J., Glover, J.E., Groves, D.I., 1979. Sedimentary evidence for an Archaean shallow-water volcanic-sedimentary facies, Eastern Pilbara Block. Western Australia. Earth Planet. Sci. Lett. 43, 74–84. https://doi.org/10.1016/0012-821X(79)90156-0.

Baumgartner, R.J., van Kranendonk, M.J., Wacey, D., Fiorentini, M.L., Saunders, M., Caruso, S., Pages, A., Homann, M., Guagliardo, P., 2019. Nano−porous pyrite and organic matter in 3.5-billion-year-old stromatolites record primordial life. Geology 47, 1039–1043. https://doi.org/10.1130/G46365.1.

Baumgartner, R.J., Caruso, S., Fiorentini, M.L., van Kranendonk, M.J., Martin, L., Jeon, H., Pagès, A., Wacey, D., 2020. Sulfidization of 3.48 billion-year-old stromatolites of the Dresser Formation, Pilbara Craton: Constraints from in-situ sulfur isotope analysis of pyrite. Chem. Geol. 538, 119488 https://doi.org/10.1016/j.chemgeo.2020.119488.

Berndt, M.E., Allen, D.E., Seyfried, W.E., 1996. Reduction of CO_2 during serpentinization of olivine at 300 °C and 500 bar. Geology 24, 351. https://doi.org/10.1130/0091-7613(1996)024<0351:ROCDSO>2.3.CO;2.

Beyssac, O., Goffé, B., Chopin, C., Rouzaud, J.N., 2002. Raman spectra of carbonaceous material in metasediments: a new geothermometer. J. Metamorph. Geol. 20, 859–871. https://doi.org/10.1046/j.1525-1314.2002.00408.x.

Brasier, M.D., Green, O.R., Jephcoat, A.P., Kleppe, A.K., van Kranendonk, M.J., Lindsay, J.F., Steele, A., Grassineau, N.V., 2002. Questioning the evidence for Earth's oldest fossils. Nature 416, 76–81. https://doi.org/10.1038/416076a.

Brasier, M., Green, O., Lindsay, J., McLoughlin, N., Steele, A., Stoakes, C., 2005. Critical testing of Earth's oldest putative fossil assemblage from the ~3.5Ga Apex chert, Chinaman Creek. Western Australia. Precambrian Res. 140, 55–102. https://doi.org/10.1016/j.precamres.2005.06.008.

Brocks, J.J., 2011. Millimeter-scale concentration gradients of hydrocarbons in Archean shales: Live-oil escape or fingerprint of contamination? Geochim. Cosmochim. Acta 75, 3196–3213. https://doi.org/10.1016/j.gca.2011.03.014.

Brocks, J.J., Love, G.D., Snape, C.E., Logan, G.A., Summons, R.E., Buick, R., 2003. Release of bound aromatic hydrocarbons from late Archean and Mesoproterozoic kerogens via hydropyrolysis. Geochim. Cosmochim. Acta 67, 1521–1530. https://doi.org/10.1016/S0016-7037(02)01302-9.

Buick, R., Dunlop, J.S.R., 1990. Evaporitic sediments of Early Archaean age from the Warrawoona Group, North Pole, Western Australia. Sedimentology 37, 247–277. https://doi.org/10.1111/j.1365-3091.1990.tb00958.x.

Cao, X., Yang, J., Mao, J., 2013. Characterization of kerogen using solid-state nuclear magnetic resonance spectroscopy: A review. Int. J. Coal Geol. 108, 83–90. https://doi.org/10.1016/j.coal.2011.12.001.

Charlou, J., Donval, J., Fouquet, Y., Jean-Baptiste, P., Holm, N., 2002. Geochemistry of high H2 and CH4 vent fluids issuing from ultramafic rocks at the Rainbow hydrothermal field (36°14′N, MAR). Chem. Geol. 191, 345–359. https://doi.org/10.1016/S0009-2541(02)00134-1.

Chernov, A.A., 1984. Modern Crystallography III: Crystal Growth. Springer, Berlin, Heidelberg, p. 517.

De Gregorio, B.T., Sharp, T.G., Rushdi, A.I., Simoneit, B.R.T. (Eds.), 2011. Bugs or Gunk? Nanoscale Methods for Assessing the Biogenicity of Ancient Microfossils and Organic Matter. Springer.

Delarue, F., Rouzaud, J.-N., Derenne, S., Bourbin, M., Westall, F., Kremer, B., Sugitani, K., Deldicque, D., Robert, F., 2016. The Raman-Derived Carbonization Continuum: A Tool to Select the Best Preserved Molecular Structures in Archean Kerogens. Astrobiology 16, 407–417. https://doi.org/10.1089/ast.2015.1392.

Des Marais, D.J., Moore, J.G., 1984. Carbon and its isotopes in mid-oceanic basaltic glasses. Earth Planet. Sci. Lett. 69, 43–57. https://doi.org/10.1016/0012-821X(84)90073-6.

Djokic, T., van Kranendonk, M.J., Campbell, K.A., Walter, M.R., Ward, C.R., 2017. Earliest signs of life on land preserved in ca. 3.5 Ga hot spring deposits. Nat. Commun. 8, 15263. https://doi.org/10.1038/ncomms15263.

Djokic, T., van Kranendonk, M.J., Campbell, K.A., Havig, J.R., Walter, M.R., Guido, D.M., 2021. A Reconstructed Subaerial Hot Spring Field in the ~3.5 Billion-Year-Old Dresser Formation, North Pole Dome, Pilbara Craton. Western Australia. Astrobiology 21, 1–38. https://doi.org/10.1089/ast.2019.2072.

Duda, J.-P., Thiel, V., Bauersachs, T., Mißbach, H., Reinhardt, M., Schäfer, N., van Kranendonk, M.J., Reitner, J., 2018. Ideas and perspectives: hydrothermally driven redistribution and sequestration of early Archaean biomass – the "hydrothermal pump hypothesis". Biogeosciences 15, 1535–1548. https://doi.org/10.5194/bg-15-1535-2018.

Dunlop, J.S.R., Groves, D.I., 1978. Archean evaporitic sulfates from north pole barite deposits, Pilbara Block. Western-Australia. Econ. Geol. 73, 1390–1391.

French, K.L., Hallmann, C., Hope, J.M., Schoon, P.L., Zumberge, J.A., Hoshino, Y., Peters, C.A., George, S.C., Love, G.D., Brocks, J.J., Buick, R., Summons, R.E., 2015. Reappraisal of hydrocarbon biomarkers in Archean rocks. PNAS 112, 5915–5920. https://doi.org/10.1073/pnas.1419563112.

Gourier, D., Binet, L., Calligaro, T., Cappelli, S., Vezin, H., Bréhéret, J., Hickman-Lewis, K., Gautret, P., Foucher, F., Campbell, K., Westall, F., 2019. Extraterrestrial organic matter preserved in 3.33 Ga sediments from Barberton. South Africa. Geochim. Cosmochim. Acta 258, 207–225. https://doi.org/10.1016/j.gca.2019.05.009.

Griffith, E.M., Paytan, A., 2012. Barite in the ocean - occurrence, geochemistry and palaeoceanographic applications. Sedimentology 59, 1817–1835. https://doi.org/10.1111/j.1365-3091.2012.01327.x.

Hahn, E.L., 1950. Spin Echoes. Phys. Rev. 80, 580–594. https://doi.org/10.1103/PhysRev.80.580.

Hanor, J.S., 2000. Barite-Celestine Geochemistry and Environments of Formation. Rev. Mineral Geochem. 40, 193–275. https://doi.org/10.2138/rmg.2000.40.4.

Harris, A.C., White, N.C., McPhie, J., Bull, S.W., Line, M.A., Skrzeczynski, R., Mernagh, T. P., Tosdal, R.M., 2009. Early Archean Hot Springs above Epithermal Veins, North Pole, Western Australia: New Insights from Fluid Inclusion Microanalysis. Econ. Geol. 104, 793–814. https://doi.org/10.2113/gsecongeo.104.6.793.

Hawkes, J.A., Hansen, C.T., Goldhammer, T., Bach, W., Dittmar, T., 2016. Molecular alteration of marine dissolved organic matter under experimental hydrothermal conditions. Geochim. Cosmochim. Acta 175, 68–85. https://doi.org/10.1016/j.gca.2015.11.025.

Hickman, A.H., 1983. Geology of the Pilbara Block and its environs: Western Australia. Bull, U.S. Geol. Surv., p. 268

Hickman-Lewis, K., Cavalazzi, B., Sorieul, S., Gautret, P., Foucher, F., Whitehouse, M.J., Jeon, H., Georgelin, T., Cockell, C.S., Westall, F., 2020. Metallomics in deep time and the influence of ocean chemistry on the metabolic landscapes of Earth's earliest ecosystems. Sci. Rep. 10, 4965. https://doi.org/10.1038/s41598-020-61774-w.

Holburg, J., Müller, M., Mann, K., Wild, P., Eusterhues, K., Thieme, J., 2022. High-Resolution Table-Top NEXAFS Spectroscopy. Anal. Chem. 94, 3510–3516. https://doi.org/10.1021/acs.analchem.1c04374.

Horita, J., Berndt, M.E., 1999. Abiogenic methane formation and isotopic fractionation under hydrothermal conditions. Science 285, 1055–1057. https://doi.org/10.1126/science.285.5430.1055.

Igisu, M., Takahashi, Y., Uematsu, K., Takeichi, Y., Ueno, Y., Takai, K., 2022. STXM-XANES analyses of carbonaceous matter in seafloor hydrothermal deposits from the ~3.5 Ga Dresser Formation in the North Pole area. Western Australia. Geochem. J. 56, 129–133. https://doi.org/10.2343/geochemj.GJ22010.

Kouketsu, Y., Mizukami, T., Mori, H., Endo, S., Aoya, M., Hara, H., Nakamura, D., Wallis, S., 2014. A new approach to develop the Raman carbonaceous material geothermometer for low-grade metamorphism using peak width. Isl. Arc 23, 33–50. https://doi.org/10.1111/iar.12057.

Lepot, K., 2020. Signatures of early microbial life from the Archean (4 to 2.5 Ga) eon. Earth Sci. Rev. 209, 103296 https://doi.org/10.1016/j.earscirev.2020.103296.

Lepot, K., Williford, K.H., Ushikubo, T., Sugitani, K., Mimura, K., Spicuzza, M.J., Valley, J.W., 2013. Texture-specific isotopic compositions in 3.4Gyr old organic matter support selective preservation in cell-like structures. Geochim. Cosmochim. Acta 112, 66–86. https://doi.org/10.1016/j.gca.2013.03.004.

Lin, H.-T., Butterfield, D.A., Baker, E.T., Resing, J.A., Huber, J.A., Cowen, J.P., 2021. Organic Biogeochemistry in West Mata, NE Lau Hydrothermal Vent Fields. Geochem. Geophys. 22 https://doi.org/10.1029/2020GC009481.

Lindsay, J.F., Brasier, M.D., McLoughlin, N., Green, O.R., Fogel, M., Steele, A., Mertzman, S.A., 2005. The problem of deep carbon—An Archean paradox. Precambrian Res. 143, 1–22. https://doi.org/10.1016/j.precamres.2005.09.003.

Love, G.D., Snape, C.E., Carr, A.D., Houghton, R.C., 1995. Release of covalently-bound alkane biomarkers in high yields from kerogen via catalytic hydropyrolysis. Org. Geochem. 23, 981–986. https://doi.org/10.1016/0146-6380(95)00075-5.

Marshall, C.P., Love, G.D., Snape, C.E., Hill, A.C., Allwood, A.C., Walter, M.R., van Kranendonk, M.J., Bowden, S.A., Sylva, S.P., Summons, R.E., 2007. Structural characterization of kerogen in 3.4Ga Archaean cherts from the Pilbara Craton. Western Australia. Precambrian Res. 155, 1–23. https://doi.org/10.1016/j.precamres.2006.12.014.

McCollom, T.M., Ritter, G., Simoneit, B.R., 1999. Lipid synthesis under hydrothermal conditions by Fischer-Tropsch-type reactions. Orig. Life Evol. Biosph. 29, 153–166. https://doi.org/10.1023/a:1006592502746.

McCollom, T., Seewald, J., 2006. Carbon isotope composition of organic compounds produced by abiotic synthesis under hydrothermal conditions. Earth Planet. Sci. Lett. 243, 74–84. https://doi.org/10.1016/j.epsl.2006.01.027.

McCollom, T.M., Seewald, J.S., 2007. Abiotic synthesis of organic compounds in deep-sea hydrothermal environments. Chem. Rev. 107, 382–401. https://doi.org/10.1021/cr0503660.

Meredith, W., Russell, C.A., Cooper, M., E. Snape, C., Love, G.D., Fabbri, D., Vane, C.H., 2004. Trapping hydropyrolysates on silica and their subsequent thermal desorption to facilitate rapid fingerprinting by GC–MS. Org. Geochem. 35, 73–89. 10.1016/j.orggeochem.2003.07.002.

Meredith, W., Snape, C.E., Love, G.D. (Eds.), 2014. Development and Use of Catalytic Hydropyrolysis (HyPy) as an Analytical Tool for Organic Geochemical Applications. Royal Society of Chemistry.

Miknis, F.P., Sullivan, M., Bartuska, V.J., Maciel, G.E., 1981. Cross-polarization magic-angle spinning 13C NMR spectra of coals of varying rank. Org. Geochem. 3, 19–28. https://doi.org/10.1016/0146-6380(81)90009-7.

Mißbach, H., Duda, J.-P., Lünsdorf, N.K., Schmidt, B.C., Thiel, V., 2016. Testing the preservation of biomarkers during experimental maturation of an immature kerogen. Int. J. Astrobiology 15, 165–175. https://doi.org/10.1017/S1473550416000069.

Mißbach, H., Schmidt, B.C., Duda, J.-P., Lünsdorf, N.K., Goetz, W., Thiel, V., 2018. Assessing the diversity of lipids formed via Fischer-Tropsch-type reactions. Org. Geochem. 119, 110–121. https://doi.org/10.1016/j.orggeochem.2018.02.012.

Mißbach, H., Duda, J.-P., van den Kerkhof, A.M., Lüders, V., Pack, A., Reitner, J., Thiel, V., 2021. Ingredients for microbial life preserved in 3.5 billion-year-old fluid inclusions. Nat. Commun. 12, 1101. https://doi.org/10.1038/s41467-021-21323-z.

Morag, N., Williford, K.H., Kitajima, K., Philippot, P., van Kranendonk, M.J., Lepot, K., Thomazo, C., Valley, J.W., 2016. Microstructure-specific carbon isotopic signatures of organic matter from ~3.5 Ga cherts of the Pilbara Craton support a biologic origin. Precambrian Res. 275, 429–449. https://doi.org/10.1016/j.precamres.2016.01.014.

Nemchin, A.A., Whitehouse, M.J., Menneken, M., Geisler, T., Pidgeon, R.T., Wilde, S.A., 2008. A light carbon reservoir recorded in zircon-hosted diamond from the Jack Hills. Nature 454, 92–95. https://doi.org/10.1038/nature07102.

Nijman, W., de Bruijne, K.H., Valkering, M.E., 1998. Growth fault control of Early Archaean cherts, barite mounds and chert-barite veins, North Pole Dome, Eastern Pilbara. Western Australia. Precambrian Res. 88, 25–52. https://doi.org/10.1016/S0301-9268(97)00062-4.

Olcott Marshall, A., Emry, J.R., Marshall, C.P., 2012. Multiple generations of carbon in the apex chert and implications for preservation of microfossils. Astrobiology 12, 160–166. https://doi.org/10.1089/ast.2011.0729.

Pearson, A. (Ed.), 2010. Pathways of carbon assimilation and their impact on organic matter values $\delta^{13}C$. Timmis, K.N. (Ed.), Handbook of Hydrocarbon and Lipid Microbiology, Springer, Berlin.

Philippot, P., van Zuilen, M., Lepot, K., Thomazo, C., Farquhar, J., van Kranendonk, M.J., 2007. Early Archaean microorganisms preferred elemental sulfur, not sulfate. Science 317, 1534–1537. https://doi.org/10.1126/science.1145861.

Preuß, A., Schauder, R., Fuchs, G., Stichler, W., 1989. Carbon isotope fractionation by autotrophic bacteria with three different CO_2 fixation pathways. Z. Naturforschung c.

Proskurowski, G., Lilley, M.D., Seewald, J.S., Früh-Green, G.L., Olson, E.J., Lupton, J.E., Sylva, S.P., Kelley, D.S., 2008. Abiogenic hydrocarbon production at lost city hydrothermal field. Science 319, 604–607. https://doi.org/10.1126/science.1151194.

Rasmussen, B., Buick, R., 1999. Redox state of the Archean atmosphere: Evidence from detrital heavy minerals in ca. 3250–2750 Ma sandstones from the Pilbara Craton, Australia. Geology 27, 115. https://doi.org/10.1130/0091-7613(1999)027<0115:RSOTAA>2.3.CO;2.

Rasmussen, B., Fletcher, I.R., Brocks, J.J., Kilburn, M.R., 2008. Reassessing the first appearance of eukaryotes and cyanobacteria. Nature 455, 1101–1104. https://doi.org/10.1038/nature07381.

Rasmussen, B., Muhling, J.R., 2023. Organic carbon generation in 3.5-billion-year-old basalt-hosted seafloor hydrothermal vent systems. Sci. Adv. 9, eadd7925. https://doi.org/10.1126/sciadv.add7925.

Reinhardt, M., Goetz, W., Duda, J.-P., Heim, C., Reitner, J., Thiel, V., 2019. Organic signatures in Pleistocene cherts from Lake Magadi (Kenya) – implications for early Earth hydrothermal deposits. Biogeosciences 16, 2443–2465. https://doi.org/10.5194/bg-16-2443-2019.

Reinhardt, M., Thiel, V., Duda, J.-P., Hofmann, A., Bajnai, D., Goetz, W., Pack, A., Reitner, J., Schanofski, M., Schönig, J., Whitehouse, M.J., Drake, H., 2024. Aspects of the biological carbon cycle in a ca. 3.42-billion-year-old marine ecosystem. Precambrian Res. 402, 107289 https://doi.org/10.1016/j.precamres.2024.107289.

Rouillard, J., van Kranendonk, M.J., Lalonde, S., Gong, J., van Zuilen, M.A., 2021. Correlating trace element compositions, petrology, and Raman spectroscopy data in the ~3.46 Ga Apex chert, Pilbara Craton, Australia. Precambrian Res. 366, 106415 https://doi.org/10.1016/j.precamres.2021.106415.

Runge, E.A., Duda, J.-P., van Kranendonk, M.J., Reitner, J., 2022a. Earth's oldest tsunami deposit? Early Archaean high-energy sediments in the ca 3.48 Ga Dresser Formation (Pilbara, Western Australia). Depos. Rec. 8, 590–602. https://doi.org/10.1002/dep2.175.

Runge, E.A., Mansor, M., Kappler, A., Duda, J.-P., 2022b. Microbial biosignatures in ancient deep-sea hydrothermal sulfides. Geobiology. https://doi.org/10.1111/gbi.12539.

Runnegar, B., Dollase, W.A., Ketcham, R.A., Colbert, M., Carlson, W.D. (Eds.), 2001. Early Archean Sulfates from Western Australia First Formed as Hydrothermal Barites Not Gypsum Evaporites. Geological Society of America, Annual Meeting and Exposition Abstracts.

Rushdi, A.I., Simoneit, B.R., 2001. Lipid formation by aqueous Fischer-Tropsch-type synthesis over a temperature range of 100 to 400 degrees C. Orig. Life Evol. Biosph. 31, 103–118. https://doi.org/10.1023/A:1006702503954.

Sakata, S., Hayes, J.M., McTaggart, A.R., Evans, R.A., Leckrone, K.J., Togasaki, R.K., 1997. Carbon isotopic fractionation associated with lipid biosynthesis by a cyanobacterium: relevance for interpretation of biomarker records. Geochim. Cosmochim. Acta 61, 5379–5389. https://doi.org/10.1016/S0016-7037(97)00314-1.

Sangély, L., Chaussidon, M., Michels, R., Huault, V., 2005. Microanalysis of carbon isotope composition in organic matter by secondary ion mass spectrometry. Chem. Geol. 223, 179–195. https://doi.org/10.1016/j.chemgeo.2005.06.001.

Schidlowski, M., 1988. A 3,800-million-year isotopic record of life from carbon in sedimentary rocks. Nature 333, 313–318. https://doi.org/10.1038/333313a0.

Sephton, M.A., 2002. Organic compounds in carbonaceous meteorites. Nat. Prod. Rep. 19, 292–311. https://doi.org/10.1039/B103775G.

Sforna, M.C., van Zuilen, M.A., Philippot, P., 2014. Structural characterization by Raman hyperspectral mapping of organic carbon in the 3.46 billion-year-old Apex chert. Western Australia. Geochim. Cosmochim. Acta 124, 18–33. https://doi.org/10.1016/j.gca.2013.09.031.

Shock, E.L., Schulte, M.D., 1998. Organic synthesis during fluid mixing in hydrothermal systems. J. Geophys. Res. 103, 28513–28527. https://doi.org/10.1029/98JE02142.

Shtukenberg, A.G., Ward, M.D., Kahr, B., 2017. Crystal Growth with Macromolecular Additives. Chem. Rev. 117, 14042–14090. https://doi.org/10.1021/acs.chemrev.7b00285.

Terabayashi, M., Masada, Y., Ozawa, H., 2003. Archean ocean-floor metamorphism in the North Pole area, Pilbara Craton. Western Australia. Precambrian Res. 127, 167–180. https://doi.org/10.1016/S0301-9268(03)00186-4.

Thakur, R.S., Kurur, N.D., Madhu, P.K., 2006. Swept-frequency two-pulse phase modulation for heteronuclear dipolar decoupling in solid-state NMR. Chem. Phys. Lett. 426, 459–463. https://doi.org/10.1016/j.cplett.2006.06.007.

Tice, M.M., Bostick, B.C., Lowe, D.R., 2004. Thermal history of the 3.5–3.2 Ga Onverwacht and Fig Tree Groups, Barberton greenstone belt, South Africa, inferred by Raman microspectroscopy of carbonaceous material. Geology 32, 37. https://doi.org/10.1130/G19915.1.

Tissot, B.P., Welte, D.H., 1984. Petroleum Formation and Occurrence.: From Kerogen to Petroleum. Springer.

Ueno, Y., Yoshioka, H., Maruyama, S., Isozaki, Y., 2004. Carbon isotopes and petrography of kerogens in ~3.5-Ga hydrothermal silica dikes in the North Pole area. Western Australia. Geochim. Cosmochim. Acta 68, 573–589. https://doi.org/10.1016/S0016-7037(03)00462-9.

Ueno, Y., 2007. Earth's Oldest Rocks: Stable Carbon and Sulfur Isotope Geochemistry of the ca. 3490 Ma Dresser Formation Hydrothermal Deposit, Pilbara Craton, Western. Developments in Precambrian Geology.

van Kranendonk, M.J., 2006. Volcanic degassing, hydrothermal circulation and the flourishing of early life on Earth: A review of the evidence from c. 3490–3240 Ma rocks of the Pilbara Supergroup, Pilbara Craton. Western Australia. Earth Sci. Rev. 74, 197–240. https://doi.org/10.1016/j.earscirev.2005.09.005.

van Kranendonk, M.J., Hickman, A.H., Williams, I.R., Nijman, W. (Eds.), 2001. Archaean geology of the East Pilbara granite-greenstone terrane, Western Australia—a field guide, 2001st ed.

van Kranendonk, M.J., Djokic, T., Poole, G., Tadbiri, S., Steller, L., Baumgartner, R. (Eds.), 2018. Depositional Setting of the Fossiliferous, c.3480 Ma Dresser Formation, Pilbara Craton. Earth's Oldest Rocks.

van Kranendonk, M.J., Philippot, P., Lepot, K., Bodorkos, S., Pirajno, F., 2008. Geological setting of Earth's oldest fossils in the ca. 3.5Ga Dresser Formation, Pilbara Craton. Western Australia. Precambrian Res. 167, 93–124. https://doi.org/10.1016/j.precamres.2008.07.003.

van Kranendonk, M.J., Pirajno, F., 2004. Geochemistry of metabasalts and hydrothermal alteration zones associated with c. 3.45 Ga chert and barite deposits: implications for the geological setting of the Warrawoona Group, Pilbara Craton, Australia. Geochem.: Explor. Environ. Anal. 4, 253–278. https://doi.org/10.1144/1467-7873/04-205.

van Kranendonk, M.J. (Ed.), 2007. Chapter 7.2 A Review of the Evidence for Putative Paleoarchean Life in the Pilbara Craton, Western Australia. Developments in Precambrian Geology.

van Kranendonk, M.J. (Ed.), 2011. Morphology as an Indictor of Biogenicity for 3.5–3.2 Ga Fossil Stromatolites from the Pilbara Craton, Western Australia. Advances in Stromatolite Geobiology.

van Zuilen, M.A., Chaussidon, M., Rollion-Bard, C., Marty, B., 2007. Carbonaceous cherts of the Barberton Greenstone Belt, South Africa: Isotopic, chemical and structural characteristics of individual microstructures. Geochim. Cosmochim. Acta 71, 655–669. https://doi.org/10.1016/j.gca.2006.09.029.

Vandenbroucke, M., Largeau, C., 2007. Kerogen origin, evolution and structure. Org. Geochem. 38, 719–833. https://doi.org/10.1016/j.orggeochem.2007.01.001.

Walter, M.R., Buick, R., Dunlop, J.S.R., 1980. Stromatolites 3400–3500 Myr old from the North Pole area, Western Australia. Nature 284, 443–445. https://doi.org/10.1038/284443a0.

Welin, E., 1966. The Occurrence of Asphaltite and Thucholite in the Precambrian Bedrock of Sweden. Geol. Fören. Stockh. Förh. 87, 509–526. https://doi.org/10.1080/11035896609448319.